2002

Modeling of Constriction Resistance in Coated Joints

E. L. Olsen

S V. Garimella
Purdue University, sureshg@purdue.edu

C. V. Madhusudana

MODELING OF CONSTRICTION RESISTANCE IN COATED JOINTS[¶]

Erik L. Olsen, Suresh V. Garimella[§]
School of Mechanical Engineering
Purdue University
West Lafayette, Indiana 47907-1288 USA

and C. V. Madhusudana
School of Mechanical and Manufacturing Engineering
University of New South Wales
Sydney 2052 Australia

Abstract

Metallic coatings applied to surfaces in contact have been shown to be effective at reducing thermal contact resistance. Contact resistance is primarily caused by the constriction of heat flow as it passes through individual contact spots. Most analyses of coated constrictions have been limited to plane contacts of a semi-infinite cylinder, while an actual constriction terminates in a shape like the frustum of a cone. A numerical model has been developed to determine the constriction resistance of such a coated asperity. The gap between the cone and contact surface is considered to either be evacuated or filled with a gas, and the temperature jump phenomenon is included in the gas-gap model. The effects of radiation heat transfer are also included. The results indicate that an optimum coating thickness for minimizing constriction resistance exists in all cases. Most gases are found to reduce the coating effectiveness very slightly, especially compared to the effect of radiation. The effect of radiation on the model is shown to be highly dependent on the joint temperature, substrate and coating thermal conductivities, and constriction ratio. Contrary to current belief, radiation is shown to be important even for temperatures below 300°C when either the substrate conductivity or the constriction ratio is very low.

[¶] *AIAA Journal of Thermophysics and Heat Transfer*, Vol. 16, No. 2, 2002.

[§] Contact person: (765) 494-5621, sureshg@ecn.purdue.edu

Nomenclature

a	Contact spot radius
A	Cylinder cross-sectional area
b	heat flux tube radius
D	z coordinate of frustum of cone
g	Temperature jump distance
G	Geometric constriction resistance amplification factor
i	Radial mesh coordinate
j	Axial mesh coordinate
L	Cylinder length
n	Normal direction
r	Radial coordinate
R	Thermal resistance
t	Coating thickness
T	Temperature
z	Axial coordinate

Greek Symbols

α	Thermal accommodation coefficient
η	Constriction resistance reduction factor
ε_c	Coating emissivity
ε_s	Substrate emissivity
ϕ	Coating projection angle
θ	Cone angle
Ψ	Constriction alleviation factor
ΔT	Temperature difference, $T_1 - T_0$

Subscripts and Superscripts

*	Extrapolated
′	Predicted
0	Asperity tip (z = 0)

1	Asperity top (z = L)
bulk	Bulk
c	Coating material
con	Constriction
cyl	Semi-infinite cylinder
eff	Effective
g	Gas material
semi-∞	Half-space
I	Interface
s	Substrate material

Introduction

The reduction of thermal contact resistance is an important research area in microelectronics [1], avionics and space applications. The imperfect contact between any two solid surfaces creates a resistance to heat flow, manifested as a temperature drop across the interface. This resistance is a major barrier to the removal of heat dissipated by electronic components, and the resulting overheating can cause performance degradation, and ultimately, failure. The first step in predicting the contact resistance of a joint is to determine the constriction resistance associated with an individual contact spot. The purpose of this work is to study the effect of metallic coatings on the constriction resistance at an individual contact point. This work considers the effects of conduction through the solid contact spot, as well as the effects of conduction through the surrounding interstitial gas and radiation heat transfer.

Experimental work has shown that metallic coatings effectively reduce thermal contact resistance. Much of this work has been reviewed by Madhusudana [2] and Lambert and Fletcher [3]. Desirable coatings are generally soft, highly conductive metals deposited on one or both contact surfaces. Commonly studied metals include copper, gold, indium, lead, nickel, silver and tin. Optimum coating thicknesses have been found for each material [2,3]. Most researchers

identified the ratio of thermal conductivity to microhardness as the most important factor in affecting the thermal contact conductance. These coatings are beneficial both because of their softness, which allows them to fill in some of the interstitial gaps under loading, and their higher conductivity, which poses a smaller resistance to heat flow through the constriction. The purpose of the present study is to evaluate the latter effect, since no separate deformation analysis is performed and the coating is assumed to follow the shape of the substrate asperity.

In any real joint there are several contact spots, and the constriction and subsequent spreading of the heat flow through these spots generates a resistance. The constriction resistance is defined as

$$R_{con} = \frac{T^* - T_0}{q} \tag{1}$$

where the definitions of T^* and T_0 in a typical temperature profile are shown in Fig. 1.

An individual contact spot can be modeled as a constriction at the end of a semi-infinite cylinder, or heat flux tube, as shown in Fig. 2. Carslaw and Jaeger [4] showed that the constriction resistance of a circular area of radius a at the boundary of a semi-infinite medium with uniform temperature boundary conditions is given by:

$$R_{con,\ semi\text{-}\infty} = \frac{1}{4ka} \tag{2}$$

Mikic and Rohsenow [5] showed that the constriction resistance of a semi-infinite cylinder is proportional to that of a semi-infinite domain (half space), and defined a constriction alleviation factor representing the reduction in constriction resistance when such a cylinder is considered instead of a semi-infinite domain, such that

$$R_{con,cyl} = \Psi \cdot R_{con,semi\text{-}\infty} \tag{3}$$

Several researchers have evaluated the constriction alleviation factor for uncoated surfaces [6,7]. Cooper et al. [8] determined that the constriction alleviation factor could be adequately approximated by the expression:

$$\Psi \approx \left(1 - \frac{a}{b}\right)^{1.5} \tag{4}$$

in which a and b are defined as in Fig. 2.

A number of studies have investigated the effect of surface coatings on the constriction resistance of both a half space and a semi-infinite cylinder, generally showing that coatings of thickness twice the contact radius can dramatically reduce the constriction resistance. Most of this work, however, has been limited to a plane contact, as reviewed by Mohs et al. [9], while an actual constriction would not terminate in a plane contact, but in a shape similar to the frustum of a cone, as shown in Fig. 3. The gap surrounding the cone can be considered to be a vacuum or to contain some fluid. Madhusudana [10] found that the constriction resistance increases as the angle between the cone and the interface θ increases, and that a fluid-filled gap significantly reduces the constriction resistance, especially at low constriction ratios (a/b).

The present work improves on previous plane-contact models through the addition of three levels of sophistication. The first of the improvements in the model considers conduction through the solids only in a frustum-terminated semi-infinite cylinder. Next, conduction through an interstitial gas is added to the model. As the thickness of a real gap is on the order of 1 μm, natural convection may be neglected [2]. The incorporation into the model of this gas gap is complicated by the presence of a temperature jump. The temperature jump represents the imperfect heat exchange at a gas-solid boundary. This imperfect exchange creates an additional resistance which is seen as a "jump" in temperature near the boundary. This resistance is generally accounted for by the addition of a temperature jump distance, g, to the width of the gas gap. Kennard [11] proposed an expression for the temperature jump distance which, along with

Song and Yovanovich's correlation for thermal accommodation coefficient [12], was used to determine the temperature jump distances used in this study. The effect on the model of the addition of both conduction through the gas gap and the temperature jump are evaluated, as well as their effect on the optimum coating thickness.

Finally, the effects of radiation heat transfer are added to the model. The effect of radiation on the constriction resistance has generally been treated as negligible for joint temperatures below 300°C [2]. This widely used assumption is evaluated in the present work; the effects of including radiation on the coating effectiveness are also considered, and the optimum coating thickness when radiation is not negligible is sought. Although radiation effects have been viewed as unimportant in electronics cooling, where temperatures are generally well below 300°C, they would be significant in high-temperature applications such as nuclear reactors, stationary packed beds (such as those used for thermal energy storage), powder insulations, and catalytic converters; these applications provide the motivation for this addition.

Numerical Analysis

This work is a numerical analysis of the constriction resistance of coated and uncoated asperities, both with and without an interstitial gas, and with and without radiation heat transfer. The asperity is modeled as shown in Fig. 3, where heat flows through an insulated, semi-infinite cylinder terminating in the frustum of a cone. The semi-infinite approximation is valid if L is large enough such that the heat flux at the top boundary is uniform. The coating and substrate are assumed to have deformed identically, and any additional deformation of the coating due to differing hardnesses is neglected. The angle ϕ is dependent on the contact spot size before and after the coating is applied. In the absence of experimental data, ϕ is simply assumed to be equal to $\theta/2$.

Assuming steady-state, axisymmetric heat conduction with constant material properties in the substrate, coating, and gas, the problem is governed by the two-dimensional, steady-state heat conduction equation and boundary conditions at both asperity ends and all substrate-coating and coating-gas boundaries, as follows:

$$\frac{1}{r}\frac{\partial}{\partial r}\left(r\frac{\partial T}{\partial r}\right)+\frac{\partial^2 T}{\partial z^2}=0 \tag{5}$$

$$\frac{\partial T}{\partial r}(0,z)=0 \quad 0 \le z \le L + t \tag{6}$$

$$\frac{\partial T}{\partial r}(b,z)=0 \quad 0 \le z \le L + t \tag{7}$$

$$T(r,0)=T_0 \quad 0 \le r \le a \tag{8a}$$

$$\frac{\partial T}{\partial n}(r,D)=0 \quad a < r \le b \tag{8b}$$

$$T(r,0)=T_0 \quad 0 \le r \le b \tag{9}$$

where n is the unit vector with outward direction normal to the surface z = D, and

$$D=(r-a)\tan q \tag{10}$$

$$T(r,L+t)=T_1 \quad 0 \le r \le b \tag{11}$$

Equations (8a) and (8b) apply when the gap is a vacuum, while (9) applies when the gap is filled with gas. The entire top and bottom surfaces are assumed isothermal. For the top surface (z = L + t), this is equivalent to an isoflux condition provided that the boundary is sufficiently far from the constriction. For the bottom surface (z = 0), the isothermal assumption holds if the two sides of the constriction are symmetric, as is usually assumed. Assuming perfect contact at the coating-substrate interface, the boundary conditions at the interface are:

$$\left(k\frac{\partial T}{\partial n}\right)_s=\left(k\frac{\partial T}{\partial n}\right)_c \quad z = D_I,\ 0 \le r \le b \tag{12}$$

$$T_s = T_c \quad z = D_I,\ 0 \le r \le b \tag{13}$$

$$\begin{cases} D_I = t & 0 \le a \le r \\ D_I = t + (r-a)\tan q & a \le r \le b \end{cases} \tag{14}$$

Similarly, when the temperature jump is not included at the coating-gas interface, the boundary conditions at the interface are:

$$\left(k\frac{\partial T}{\partial n}\right)_c = \left(k\frac{\partial T}{\partial n}\right)_g \quad z = D,\ a < r \le b \tag{15}$$

$$T_c = T_g \quad z = D,\ a < r \le b \tag{16}$$

For the numerical solution, the heat conduction equation (5) was cast in terms of a second-order central difference approximation for the derivatives. Second-order approximations were also used for the domain boundaries. First-order finite difference equations for the interior boundaries were obtained by applying an energy balance on appropriate volumes.

Use of the energy balance method at the gas-coating interface also allows for the inclusion of the temperature jump phenomenon into the model. The temperature jump distance was applied in the normal direction, as the heat flow through this boundary was found to be nearly normal to the boundary when the temperature jump was not included in the model. Figure 4 shows a mesh point on the gas-coating boundary. The finite difference equation for node (i, j) can be obtained by performing an energy balance, where the distance Δr becomes ($\Delta r + g \sin \theta$) in the i direction and the distance Δz becomes ($\Delta z + g \cos \theta$) in the –j direction. Similarly, these distances are applied in the –i and +j directions for energy balances at the nodes (i, j-1) and (i+1, j). When writing these equations, the temperature jump distance is included only when it acts as a resistance, and not when calculating surface areas through which heat flows. For example, the energy balance equation at node (i, j) becomes:

$$\begin{aligned} & k_g \cdot 2\pi\left(r + \frac{\Delta r}{2}\right)\cdot \Delta z \cdot \frac{T_{i+1,j} - T_{i,j}}{\Delta r + g \cdot \sin\ ?} \quad + \quad k_g \cdot 2\pi r \cdot \Delta r \cdot \frac{T_{i,j-1} - T_{i,j}}{\Delta z + g \cdot \cos ?} \\ & + \quad k_c \cdot 2\pi\left(r - \frac{\Delta r}{2}\right)\cdot \Delta z \cdot \frac{T_{i-1,j} - T_{i,j}}{\Delta r} \quad + \quad k_c \cdot 2\pi r \cdot \Delta r \cdot \frac{T_{i,j+1} - T_{i,j}}{\Delta z} \quad = \quad 0 \end{aligned} \tag{17}$$

Radiation effects are also incorporated into the model from energy-balance considerations at the gas-coating interface. The effects of radiation are added simply by adding additional terms to Eq. (17). Figure 5 shows the surfaces participating in radiative heat transfer. Because boundary conditions (9) and (7) govern surfaces S_0 and S_1, respectively, only nodes along surface S_2 must explicitly include radiation terms in the finite difference equation.

These radiation terms were determined by evaluating the radiation contribution from the surface of each node, as shown in Fig. 6. All surfaces were assumed to be diffuse and gray. Boundary surface S_1 acts as a re-radiating surface and was assigned an emissivity of 1 along with boundary S_0. As a worst-case scenario, S_2 was also assumed to have an emissivity (ε_s) of 1 as a baseline. Boundary S_0 is at a constant temperature and hence not divided into separate nodes. The resulting finite difference equation at any given node *x* is then:

$$\text{existing energy balance terms} + \varepsilon_s \sigma \left(\sum_{j=0}^{n} A_j F_{jx} T_j^4 - A_x T_x^4 \right) = 0 \tag{18}$$

in which j and x are defined in Fig. 6. The problem reduces to that of finding each F_{jx}. Naraghi and Chung [13] developed the following expression for the view factor between the frustum of a cone and a coaxial ring:

$$F_{d'\text{-}c} = \frac{1}{\pi (1 - R_i^2)} \left\{ \begin{array}{l} -A'B' \tan^{-1}\left(\dfrac{A'C'}{B'D'} \right) + (C'D')^2 \tan^{-1} \dfrac{D'}{C'} \\ + \dfrac{\sin\alpha}{\cos^2\alpha} \left[\left(H^2 + \dfrac{2HR_i}{\tan\alpha} \right) \cdot \tan^{-1} \dfrac{(E')^{1/2}}{H} + E' \tan^{-1} \dfrac{H}{(E')^{1/2}} \right] \\ + \left(\dfrac{H^2}{2\cos^2\alpha} + HR_i \tan\alpha \right) \cos^{-1}(R_i) \end{array} \right\}$$

$$A' = \left[H^2 + (1 + H\tan\alpha + R_i)^2 \right]^{1/2} \tag{19}$$

$$B' = \left[H^2 + (1 - H\tan\alpha - R_i)^2 \right]^{1/2}$$

$$C' = (1 - R_i)^{1/2} \qquad D' = (1 + R_i)^{1/2}$$

$$E' = (1 - R_i^2)\cos^2\alpha \qquad R_i = r_i / r_o$$

where the geometry is as shown in Fig. 7. Use of this expression, together with some fairly involved view factor algebra, allows each F_{jx} to be evaluated analytically. Note that when radiation is not included in the model, only the temperature difference, ΔT, is specified, rather than an actual temperature, T_0, because all equations are linear. A numerical value for substrate thermal conductivity, k_s, is also not needed in the simpler model, since the conduction equations are only a function of the ratios k_c/k_s and k_g/k_s. Introduction of the radiation terms, however, requires actual values for T_0 and k_s to be specified.

A 201×51 element grid ($z \times r$) was used to solve the problem. A finer grid was used in the conical portion of the domain, allowing for a finer resolution in the area of high temperature gradients, and also allowing the grid spacing to be chosen such that the diagonal boundaries line up with the mesh nodes. A dedicated FORTRAN program using Gauss-Seidel iteration with successive overrelaxation [14] was used to solve the system of equations. Iterations were continued until the sum of the errors between successive iterations at all nodes was less than 0.1°C, with the temperature difference across the entire domain being 100°C. The heat flow rates through the top and bottom of the domain were also compared and agreed to within 1% for all gas-filled (no radiation) cases. This error was less than 3% for all evacuated-gap cases, most likely resulting from the higher distortion of heat flow lines near the coating-vacuum boundary in these cases, which makes the heat flow calculation at the base less accurate. The heat flux through the top of the domain was found to change by less than 1% when the grid was made twice as dense (401×101), showing that the use of the 201×51 element grid was acceptable. Also note that the coordinates r and z are nondimensional, normalized with respect to Δr and Δz, such that $r/\Delta r = 50$ and $z/\Delta z$ varies depending on the cone angle.

Definitions for Analysis of Results

In order to relate the results of this study to previous work, it is necessary to define two new terms. The first is a factor that represents the effect of frustum geometry on the constriction resistance of the uncoated asperity. The *Geometric Constriction Resistance Amplification Factor*, G, is defined as:

$$G = R_{con,q} \Big/ R_{con,cyl} = \left(\frac{T^* - T_0}{q} \right)_q \Big/ \left(\frac{T^* - T_0}{q} \right)_{cyl} \tag{20}$$

where θ is the cone angle and $R_{con,\,cyl}$ is the constriction resistance of the semi-infinite cylinder of radius b with plane-contact. The amplification factor G is always greater than unity since any non-zero angle of contact results in an increase in the geometric constriction resistance.

The second new factor represents the effect of the coating. Previous analytical studies [15] have directly calculated the constriction resistance of the substrate and the coating. The present numerical solution does not allow for such a direct calculation. However, the bulk and constriction resistances are in series such that the total resistance of the asperity is given by:

$$R_{total} = R_{s,bulk} + R_{s,con} + R_{c,bulk} + R_{c,con} \tag{21}$$

The "effective" constriction resistance of the coated asperity is the sum of the last three terms of Eq. (21). By assuming that the substrate constriction resistance accounts for any change in the isotherms in the bulk material, the substrate bulk resistance may be defined as the bulk resistance of the semi-infinite cylinder, $L/(k_s A)$. The remaining resistances then constitute an effective constriction resistance for comparison to an uncoated case, and may be calculated from:

$$R_{con,eff} = R_{s,con} + R_{c,bulk} + R_{c,con} = R_{total} - R_{s,bulk} = \frac{T_1 - T_0}{q} - \frac{L}{k_s A} \tag{22}$$

The effect of the coating can then be evaluated with the *Constriction Resistance Reduction Factor*, η, defined as the ratio of the effective constriction resistance of the coated asperity to the constriction resistance of an identical, uncoated asperity:

$$h = \frac{\left(R_{con,eff}\right)_{coated,q}}{\left(R_{con,eff}\right)_{uncoated,q}} = \frac{\left(R_{s,con} + R_{c,bulk} + R_{c,con}\right)_{coated,q}}{\left(R_{con,s}\right)_{uncoated,q}} \tag{23}$$

For all thin conductive coatings, η is less than 1, since the constriction resistance is reduced as a result of the presence of the coating. The factor η will exceed a value of 1 for very thick coatings, for which the additional bulk resistance added by the coating has a detrimental effect outweighing the reduction in constriction in the substrate. Use of these definitions allows for an expression predicting the total coated asperity resistance:

$$R'_{total} = R_{con,eff} + R_{s,bulk} = e \cdot G \cdot \Psi \cdot \frac{1}{4k_s a} + \frac{L}{k_s A} \tag{24}$$

It may be noted that, because the substrate bulk resistance is treated as a constant and is always in series with the remaining resistances, these definitions apply even when the gap is filled with gas and radiation is included. However, it is emphasized that η always represents a comparison between a coated asperity and an identical, uncoated asperity. Therefore, when the gap is gas-filled and radiation is included, it is so in both the coated and uncoated cases. The amount of bulk material remains the same in the comparison: the addition of the coating increases the total asperity length.

Results and Discussion

Initial validation of the numerical model was performed by calculation of the constriction alleviation factor for the plane contact with no coating. Results from the model are compared with the approximation suggested by Cooper et al. [8] in Table 1. The predictions agree to

within 4%. All the results presented here, with the exception of the results with radiation included, are calculated with a temperature difference of 100 K across the asperity length. The length values are not relevant; only the dimensionless length ratios L/b and a/b affect the results. The length ratio L/b is fixed at 4; this length was always found sufficient to provide isoflux conditions at the top of the domain.

Evacuated and gas-filled contact without radiation

Typical temperature contours (labeled in °C) and heat flow lines obtained from the numerical model are shown in Figs. 8 and 9, for uncoated and coated asperities with and without a gas-filled gap. There is a sharp change in the isotherms and heat flow lines at the substrate-coating boundary. More importantly, the heat flow lines are less distorted in the bulk material when the coating is added, resulting in a reduction in constriction resistance. These trends also hold for the asperities with gas-filled gaps. Because the ratio k_g/k_s for most real gas-solid combinations is very small (≤ 0.001), nearly all of the heat still flows through the solid. Only heat flow lines originating very near the outer edge of the asperity flow through the gas. Also, the heat flow at the gas-solid boundary is nearly normal to the boundary, validating the assumed direction for g, shown in Fig. 4, made when including the temperature jump in the model.

Figure 10 shows the geometric constriction resistance amplification factor G as a function of cone angle θ, for cases with and without a gas present in the gap and for several different constriction ratios. Larger values of G indicate greater constriction. As expected, G increases with increasing cone angle. Also, values of G for the gas-filled gap are lower than those for an evacuated gap, showing that the gas does alleviate some of the constriction effects. Although the variation of G with θ is monotonic with a/b for the vacuum gap, the curves for different a/b cross over for the gas-filled gap. This indicates that the sensitivity of G to θ varies for different

constriction ratios (a/b) when the gap is gas-filled, with the smaller constriction ratio being the more sensitive. This is explained by the fact that the actual size of the gap changes the most with θ for the smallest constriction ratio.

A comparison of Figs. 8(b) and 9(b) leads one to believe that the addition of the gas gap has very little effect on the coated asperity. This effect can be directly evaluated by computing the difference between heat fluxes through the coated asperity with and without the gas gap included. Figure 11 shows the percent difference between gas-filled and evacuated gap heat fluxes as a function of coating thickness. For $k_g/k_s = 0.001$, the difference is less than 3% for all constriction ratios and coating thicknesses. Only for the largest value considered in this study of $k_g/k_s = 0.01$ is there a significant change in heat flux; even in this case, the difference is less than 10% for the optimum coating thickness range of $0.3 \leq t/b \leq 0.4$. For both of these gas conductivities, the gas has the strongest effect for small constriction ratios and small coating thicknesses, as there is the largest opportunity for constriction alleviation in these cases.

Figure 12 shows the percent difference between gas-filled and evacuated gap heat fluxes for cases with and without the temperature jump considered in the model. The temperature jump distance, g, clearly has very little effect on the heat flux. As expected, the percent difference decreases slightly when the temperature jump is added because this represents an additional resistance, and hence is more similar to the vacuum case.

The effect of the coating is to decrease the constriction resistance at all constriction ratios (a/b), with the effect being more pronounced for smaller a/b, as shown in Fig. 13 for different coating thicknesses. Lower values of η indicate a decreased constriction resistance. By definition, $\eta = 1$ when the coating thickness is zero. There is an optimum coating thickness t/b for each constriction ratio at which η reaches a minimum, beyond which the additional bulk resistance introduced by the coating has a detrimental effect. This optimum thickness decreases

as the constriction ratio increases (from t/b = 0.4 at a/b = 0.1 to t/b = 0.3 at a/b = 0.4), since the constriction effects are less severe for larger a/b even without the coating. These trends hold for both the evacuated and gas-filled gaps. The inclusion of gas in the gap slightly reduces the effectiveness of the coating, again because there is a slightly smaller extent of constriction to be alleviated in these cases.

The same trends hold for higher coating conductivity ratios (k_c/k_s), with the effectiveness of the coating greatly increasing when the coating conductivity is increased from a k_c/k_s of 2 to 5. The presence of the gas gap has an even smaller effect on η at the higher conductivity ratio. In this case the optimum coating thickness is also less effective for the smaller constriction ratio (a/b) than for larger a/b, unlike the lower coating conductivity case, where the coating is always the most effective for the smallest constriction ratio.

The constriction resistance reduction factor was also seen to be a weak function of θ, and the results are not shown here. The coating was slightly more effective for large cone angles. As with G, η changed slightly more rapidly with cone angle when the gap was filled with gas, but followed the same trends. The optimum coating thickness was again in the range $0.3 \leq t/b \leq 0.4$.

Figure 14 shows η versus coating thickness for several different gas conductivity ratios (k_g/k_s). The trends previously discussed are seen to be valid at all values of gas conductivity. It is also apparent that only at very large ratios ($k_g/k_s = 0.01$), representative of combinations of low conductivity metals and high conductivity gases such as stainless steel and helium, does the presence of the gas have a large effect on η. In this case the coating is significantly less effective because the presence of the gas has already alleviated a part of the constriction effect.

Uncoated contact with radiation

Unlike the addition of the gas gap, the addition of radiation effects to the model has a significant impact on contact heat transfer. The effect of the inclusion of radiation on the constriction resistance of an uncoated asperity is discussed in this section. This is done by computing the difference between heat fluxes through the uncoated asperity with and without radiation included. The prevailing assumption that radiation is negligible below ~ 600 K would require that this difference in flux be a function of temperature only. However, the flux change due to radiation was found to be a strong function of several variables, and radiation was found to be important in many instances below 600 K, as will be shown below.

Figure 15 shows isotherms (labeled in K) and heat flow lines in a typical uncoated asperity with radiation. The addition of radiation alleviates some of the constriction by reducing the distortion of the heat flow lines near the outer edge of the asperity. Without radiation, almost all of the heat flow is completely through the solid (there will be some heat flow through the gas gap, as in Fig. 9a). With radiation, heat flow lines originating at the asperity top beyond a radius of r = 0.4 eventually pass through the asperity surface and into the gas gap, and do not undergo the extreme distortion they experience in the no-radiation case. Because of this effect, the case considered in this figure, at T_0 = 500 K, already shows that radiation may not be negligible below 600 K.

Figure 16 shows the percent difference between heat flux with and without radiation as a function of the asperity base temperature T_0. The effect of radiation on the model is a very strong function of temperature, as expected, with the difference varying between 0% at 0 K to nearly 50% at 2000 K. If a 5% change in heat flux is arbitrarily chosen as a threshold below which radiation is considered negligible, it appears that radiation may be neglected only at temperatures below 500 K for the case shown.

Moreover, the effect of radiation at different base temperatures is a strong function of the substrate thermal conductivity, as shown in Fig. 17(a). For low thermal conductivities k_s, the effect of radiation remains important at much lower temperatures – as low as 300 K when k_s = 10 W/mK. This is expected because the radiative path becomes much more favorable for heat flow as the resistance through the solid increases.

Radiation effects may also be expected to be dependent on the temperature difference across the asperity, ΔT. However, for the entire range of T_0 and k_s considered in Fig. 17(a), the heat flux variation was found to be nearly constant over the range $20\ K \le \Delta T \le 100\ K$.

The effect of radiation on the constriction resistance does depend on the asperity geometry. Figure 17(b) illustrates this dependence for several constriction ratios, a/b, and cone angles, θ. Inclusion of radiation dramatically changes the heat flux as the constriction ratio decreases. This is expected because the constriction resistance increases as the constriction ratio decreases, thus limiting heat flow through the solid and making the effects of radiation more apparent. An increase in the cone angle θ has a similar effect, as expected. The rate of variation with θ is greater at the lower constriction ratios, since a change in θ has a stronger effect on the frustum shape at lower a/b.

Finally, the effect of radiation on the constriction resistance is also a function of the surface emissivity. The difference between heat flux with and without radiation is shown as function of the substrate emissivity in Fig. 18. As expected, the effect of radiation decreases as the emissivity decreases. For values of $\varepsilon_S > 0.5$, this effect is quite small, especially compared to its variation with base temperature, substrate thermal conductivity, and constriction geometry. For values of $\varepsilon_S < 0.5$, the effect of radiation becomes increasingly unimportant.

Coated contact with radiation

Because radiation tends to alleviate the constriction resistance, it would be expected that the coating effectiveness decreases as radiation becomes more dominant, where the radiation-dominant cases are determined from results for the uncoated asperity discussed above. This is indeed generally the case, but the coating remains effective in reducing constriction resistance in all cases, and an optimum coating thickness may be identified for all cases, as was found for the cases without radiation.

Figure 19 shows heat flow lines and isotherms in a coated asperity with radiation included. As before, the coating alleviates the constriction by reducing the distortion of the heat flow lines. This effect is similar to that achieved by inclusion of radiation in the model for an uncoated asperity in Fig. 15. Hence, it is anticipated that as radiation becomes more dominant, the coating would become less effective at reducing the constriction resistance.

The constriction resistance reduction factor is shown in Fig. 20(a) as a function of coating thickness for several different base temperatures. At the smaller values of T_0, an increase in the coating thickness causes a sharp reduction in η, again reaching an optimum value of t/b followed by a gradual increase. The coating becomes dramatically less effective as T_0 increases, as radiation becomes more significant. The value for the optimum coating thickness is also seen to decrease with increasing temperature, changing from t/b = 0.35 at T_0 = 250 K to t/b = 0.20 at T_0 = 1000 K.

The coating effectiveness and optimum thickness are also strong functions of the thermal conductivities of the substrate and coating. Figure 20(b) shows the constriction resistance reduction factor as a function of coating thickness for several different substrate conductivities and two coating conductivity ratios (k_c/k_s). The coating is clearly less effective for lower substrate conductivities, again because radiation is much more dominant in low conductivity

cases. As before, the optimum coating thickness is less for the cases in which radiation is more dominant. These trends also hold at the higher coating conductivity ratios, for which the coating is again dramatically more effective. For k_s = 10 W/mK, the minimum η decreases from 0.85 for k_c/k_s = 2 to 0.20 for k_c/k_s = 5. The optimum coating thickness also increases for higher conductivity coatings.

The inclusion of radiation causes more pronounced variations in η with geometry than for the cases discussed earlier where radiation was neglected. Figure 21 shows that the coating is more effective at higher cone angles. This trend is opposite of that which would be predicted by the "radiation dominance" trend observed in Fig. 20, in which the coating became less effective when radiation was more dominant in the uncoated asperity. In this case, radiation becomes more dominant in the uncoated asperity as the cone angle increases, but the coating also becomes more effective as θ increases. However, the variation of η with θ is not nearly as strong as that with T_0 and k_s.

Figure 22 also shows an interesting trend for the variation of the coating effectiveness with a change in a/b, in the presence of radiation. At any coating thickness t/b, as the constriction ratio decreases, η first decreases and then increases again. This may be attributed to the competing effects of radiation and the constriction of heat flow in the substrate; radiation effects make the coating less effective as the constriction ratio is decreased (contribution of radiation becomes greater), whereas with a decrease in a/b, the increased constriction makes the coating more effective. This trend is also different from that observed in the earlier model without radiation, in which η decreased continuously with decreasing constriction ratio. Again, however, this variation is not nearly as strong as that with temperature and conductivity.

Variation of ΔT over the range 20 K $\leq \Delta T \leq$ 100 K was found to have nearly no effect on the constriction resistance reduction factor, as expected from the earlier results for the uncoated

asperity. Also, the variation of the factor η with emissivity was found to be very small over the range $0.6 \leq \varepsilon_c \leq 1.0$, with the maximum variation in η being only 5%. The coating becomes more effective as ε_c decreases.

Conclusions

The thermal constriction resistance of a coated asperity with both an evacuated and a gas-filled gap and with and without radiation heat transfer has been investigated by numerical solution of the steady-state heat conduction equation. The constriction resistance reduction factor, η, was introduced to aid in evaluating the effect of the coating on the constriction resistance. The trends observed for an evacuated or gas-filled gap were the same, with an optimum coating thickness identifiable for all cases. The coating is generally most effective for smaller constriction ratios, and the optimum coating thickness decreases as the constriction ratio is increased. The presence of a gas in the gap slightly reduces the constriction resistance, hence reducing the effectiveness of the coating. Inclusion of the temperature jump phenomenon was found to have a negligible effect on the results.

The extent of the effect of including radiation in the model was found to be heavily dependent on the asperity base temperature, substrate thermal conductivity, and constriction ratio. This finding is contrary to the recommendation in the literature that radiation is negligible for temperatures below 300°C for all contact resistance problems. Use of a coating was shown to still be effective at reducing the constriction resistance when radiation is introduced into the model. However, both the effectiveness and the optimum thickness of the coating were found to be highly dependent on the base temperature, substrate thermal conductivity, and coating conductivity ratio. In general, factors that tend to increase the effects of radiation on the model tend to decrease both coating effectiveness and optimum thickness.

An extension of this work will incorporate an analysis of deformation into the existing model, to account for any additional deformation in the coating over and above that of the substrate. This complete microscopic model will then be used in a macroscopic analysis that considers the effect of multiple asperities in order to predict contact resistance between real surfaces.

Acknowledgement

Support for this work from industry members of the *Purdue Cooling Technologies Research Consortium* (http://widget.ecn.purdue.edu/~CTRC) is gratefully acknowledged.

References

1. Yovanovich, M. M. and Antonetti, V. W., "Application of Thermal Contact Resistance Theory to Electronic Packages," *Advances in Thermal Modeling of Electronic Components*, Vol. 1, 1988, pp. 79-128.
2. Madhusudana, C. V., *Thermal Contact Conductance*, Springer-Verlag, New York, 1996.
3. Lambert, M.A. and Fletcher, L.S., "Review of the Thermal Contact Conductance of Junctions with Metallic Coatings and Films," *AIAA Journal of Thermophysics and Heat Transfer*, Vol. 7, 1993, pp. 547-554.
4. Carslaw, H. S. and Jaeger, J. C., *Conduction of Heat in Solids*, 2nd Ed. Clarendon Press, Oxford, 1959, pp. 214-217.
5. Mikic, B.B. and Rohsenow, W.M., "Thermal Contact Resistance," Mechanical Engineering Department Report No. DSR 74542-41, 1966, MIT, Cambridge, MA.
6. Gibson, R.D., "The Contact Resistance for a Semi-Infinite Cylinder in a Vacuum," *Applied Energy*, Vol. 2, 1976, pp. 57-65.

7. Negus, K.J., Vanoverbeke, C.A., and Yovanovich, M.M., "Thermal Constriction Resistance with Variable Conductivity near the Contact Surface," *Fundamentals of Conduction and Recent Developments in Contact Resistance*, ASME HTD-Vol. 69, 1987, pp. 91-98.
8. Cooper, M. G., Mikic, B. B. and Yovanovich, M. M., "Thermal Contact Conductance," *International Journal of Heat and Mass Transfer*, Vol. 12, 1969, pp. 279-300.
9. Mohs, W. F., Madhusudana, C. V. and Garimella, S. V., "Constriction Resistance in Coated Joints," *Proceedings of NHTC'00*, August 20-22, 2000, pp. 1-7.
10. Madhusudana, C. V., "Heat Flow Through Conical Constrictions in Vacuum and in Conducting Media," AIAA Paper 79-14071, New York, 1979.
11. Kennard, E. H., *Kinetic Theory of Gases*, McGraw-Hill, New York, pp. 311-327, 1938.
12. Song, S. and Yovanovich, M. M., "Correlation of Thermal Accommodation Coefficient for 'Engineering' Surfaces," *HTD - Fundamentals of Conduction and Recent Developments in Contact Resistance*, Vol. 69, 1987, pp. 107-116.
13. Naraghi, M. H. N. and Chung, B. T. F., "Radiation Configuration Factors Between Disks and a Class of Axisymmetric Bodies," *ASME Journal of Heat Transfer*, Vol. 104, 1982, pp. 426-431.
14. Hoffman, J. D., *Numerical Methods for Engineers and Scientists*, McGraw-Hill, New York, 1992.
15. Mikic, B. B. and Carnasciali, G., "The Effect of Thermal Conductivity of Plating Material on Thermal Contact Resistance," *ASME Journal of Heat Transfer*, Vol. 92, 1970, pp. 475-482.

FIGURE CAPTIONS

Figure 1. Typical temperature profile at a contact.

Figure 2. Semi-infinite cylinder model.

Figure 3. Frustum-terminated semi-infinite cylinder model.

Figure 4. Mesh point at gas-coating boundary.

Figure 5. Surfaces participating in radiation heat transfer.

Figure 6. Individual nodes for radiation calculation.

Figure 7. Geometry for the Naraghi-Chung expression.

Figure 8. Temperature distribution with an evacuated gap ($a/b = 0.2$, $\theta = 30°$) for (a) an uncoated asperity, and (b) a coated asperity ($t/b = 0.2$, $k_c/k_s = 5$).

Figure 9. Temperature distribution with a gas-filled gap ($a/b = 0.2$, $\theta = 30°$, $k_g/k_s = 0.001$, $g/a = 0.1$) for (a) an uncoated asperity, and (b) a coated asperity ($t/b = 0.2$, $k_c/k_s = 5$).

Figure 10. Geometric constriction resistance amplification factor versus θ.

Figure 11. Percent heat flux difference with and without gas gap for different gas conductivity ratios.

Figure 12. Percent heat flux difference with and without gas gap for cases with and without temperature jump.

Figure 13. Constriction resistance reduction factor versus coating thickness.

Figure 14. Constriction resistance reduction factor for different gas conductivity ratios.

Figure 15. Temperature distribution in uncoated asperity with radiation ($\theta = 30°$, $a/b = 0.2$, $g/a = 0.1$, $\varepsilon_s = 1.0$, $k_g/k_s = 0.001$, $k_s = 100$ W/mK, $\Delta T = 100$ K, $T_0 = 500$ K).

Figure 16. Variation with base temperature of the effect of radiation on the uncoated asperity.

Figure 17. Variation of the effect of radiation on the uncoated asperity with (a) substrate thermal conductivity, and (b) asperity geometry.

Figure 18. Variation with emissivity of the effect of radiation on the uncoated asperity.

Figure 19. Temperature distribution in coated asperity with radiation ($\theta = 30°$, $a/b = 0.2$, $g/a = 0.1$, $\varepsilon_s = 1.0$, $k_g/k_s = 0.001$, $k_s = 100$ W/mK, $\Delta T = 100$ K, $T_0 = 500$ K, $t/b = 0.3$, $k_c/k_s = 2$).

Figure 20. Variation of η versus t/b with (a) base temperature, and (b) thermal conductivities of the substrate and coating.

Figure 21. Variation of η versus t/b with cone angle.

Figure 22. Variation of η versus t/b with constriction ratio.

Table 1. Comparison of Ψ from the current numerical model with the Cooper et al. [8] approximation.

a/b	Current Model	Cooper et al.
0.1	0.8201	0.8538
0.2	0.7009	0.7155
0.3	0.5730	0.5857
0.4	0.4484	0.4648

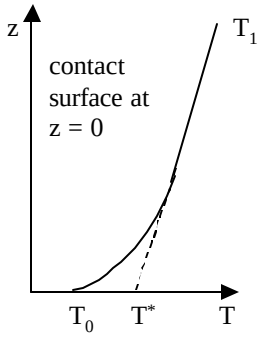

Figure 1. Typical temperature profile at a contact.

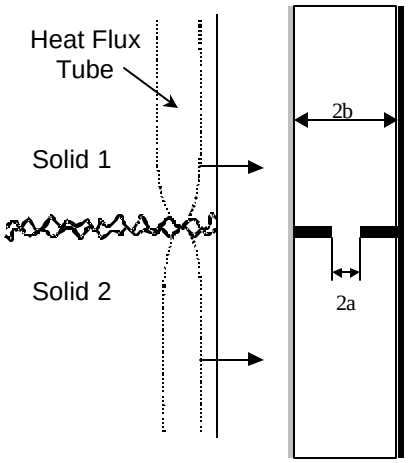

Figure 2. Semi-infinite cylinder model.

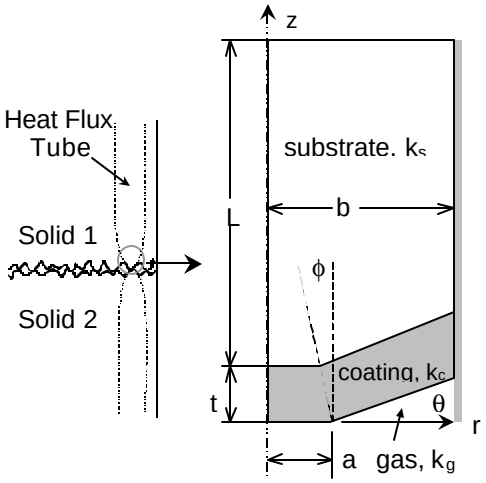

Figure 3. Frustum-terminated semi-infinite cylinder model.

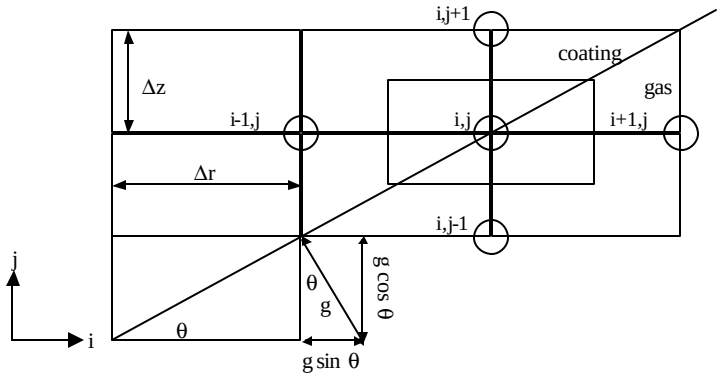

Figure 4. Mesh point at gas-coating boundary.

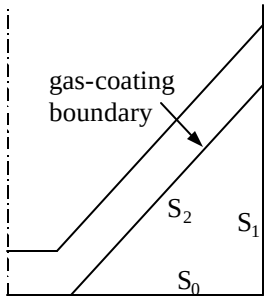

Figure 5. Surfaces participating in radiation heat transfer.

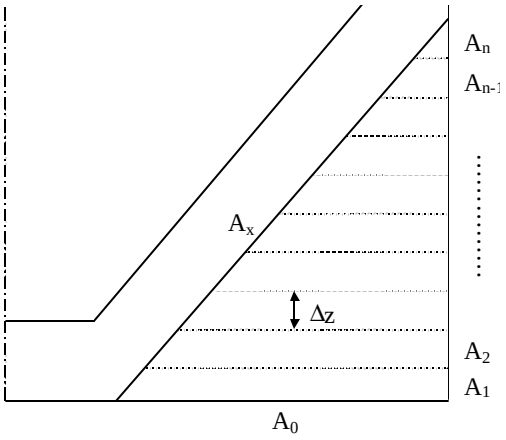

Figure 6. Individual nodes for radiation calculation.

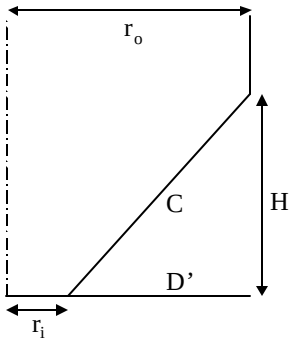

Figure 7. Geometry for the Naraghi-Chung expression.

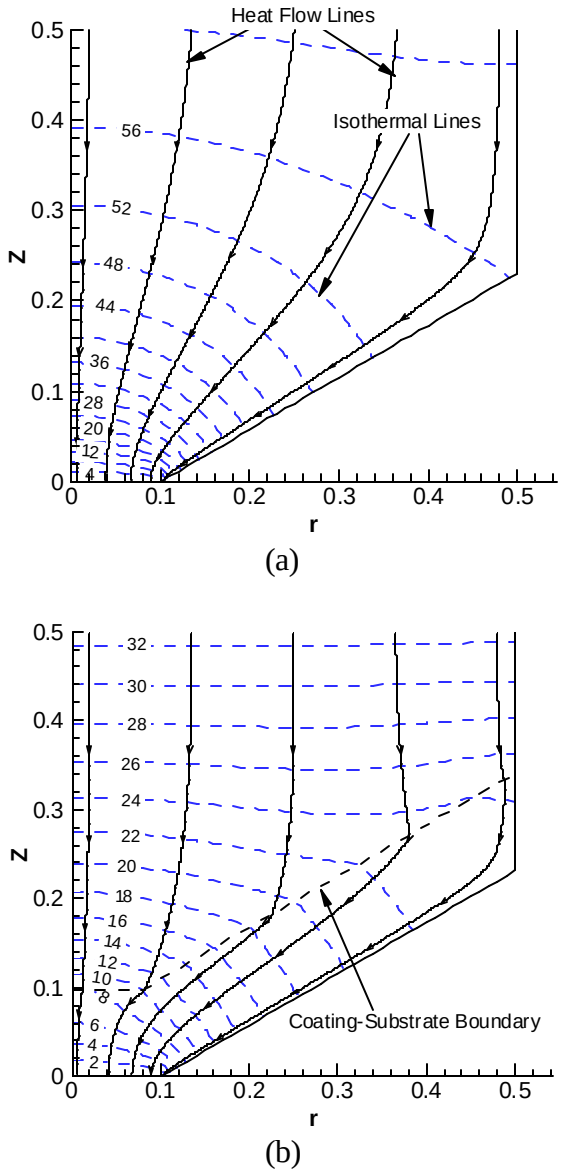

Figure 8. Temperature distribution with an evacuated gap (a/b = 0.2, θ = 30°) for (a) an uncoated asperity, and (b) a coated asperity (t/b = 0.2, k_c/k_s = 5).

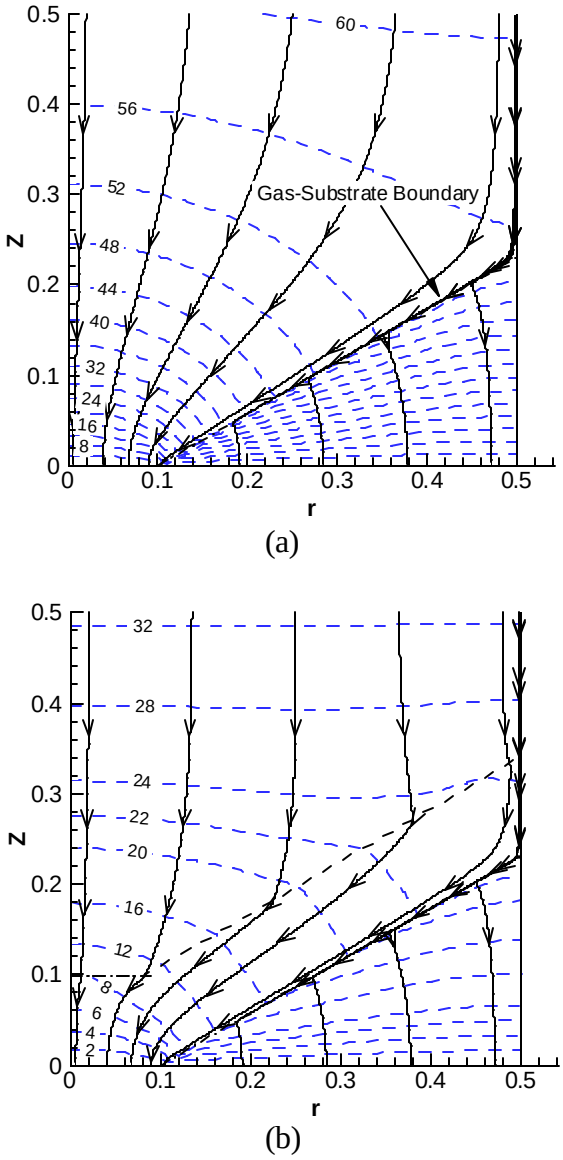

Figure 9. Temperature distribution with a gas-filled gap (a/b = 0.2, θ = 30°, k_g/k_s = 0.001, g/a = 0.1) for (a) an uncoated asperity, and (b) a coated asperity (t/b = 0.2, k_c/k_s = 5).

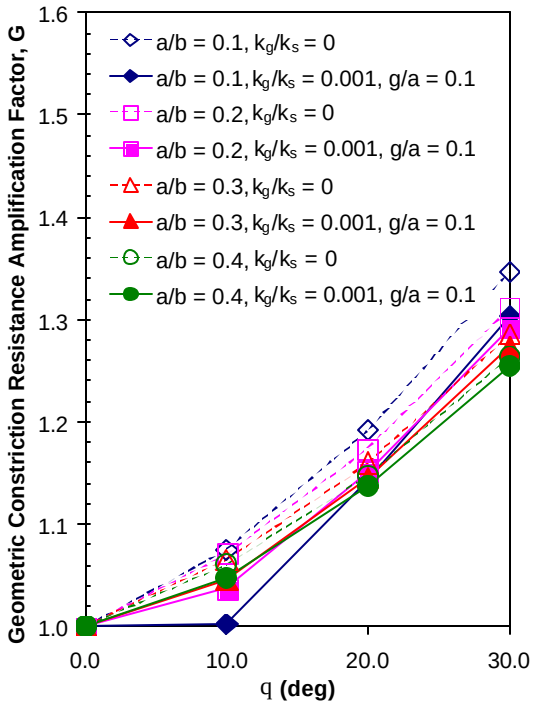

Figure 10. Geometric constriction resistance amplification factor versus θ.

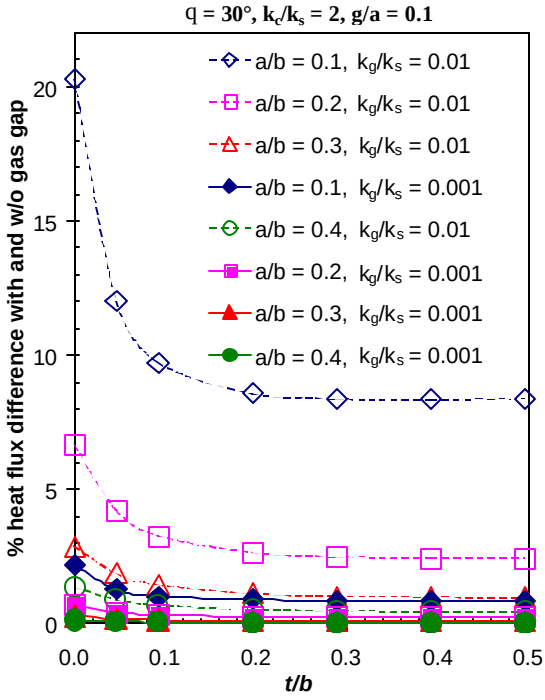

Figure 11. Percent heat flux difference with and without gas gap for different gas conductivity ratios.

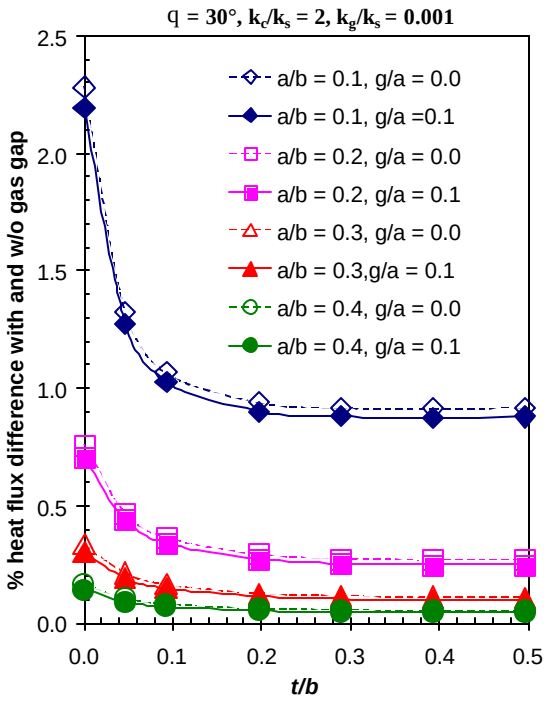

Figure 12. Percent heat flux difference with and without gas gap for cases with and without temperature jump.

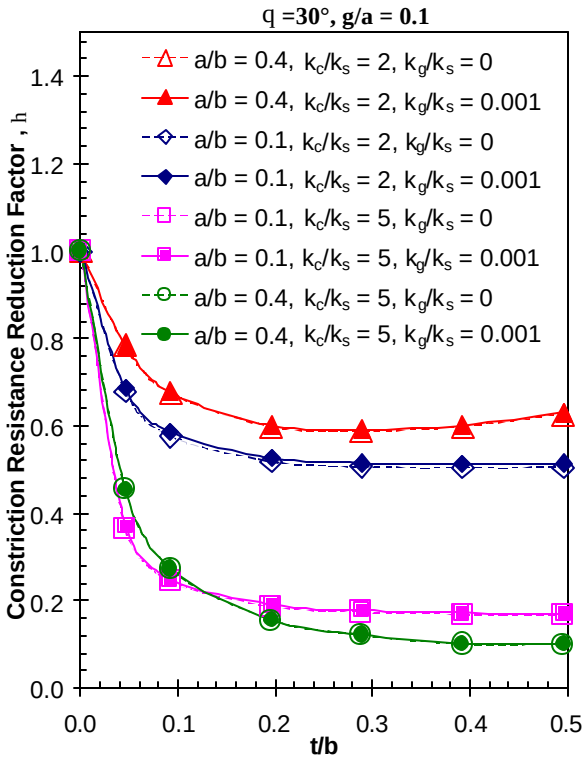

Figure 13. Constriction resistance reduction factor versus coating thickness.

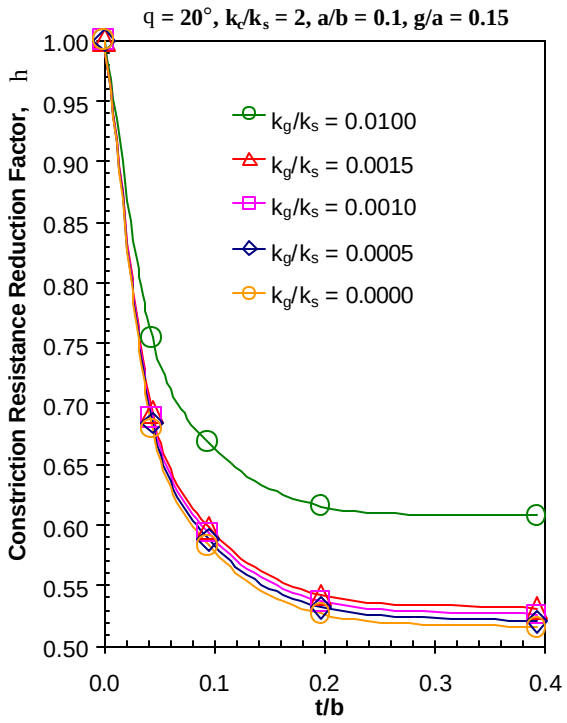

Figure 14. Constriction resistance reduction factor for different gas conductivity ratios.

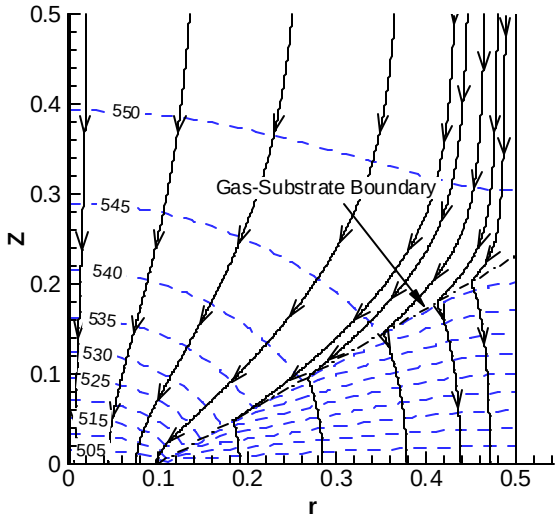

Figure 15. Temperature distribution in uncoated asperity with radiation ($\theta = 30°$, a/b = 0.2, g/a = 0.1, $\varepsilon_s = 1.0$, $k_g/k_s = 0.001$, $k_s = 100$ W/mK, $\Delta T = 100$ K, $T_0 = 500$ K).

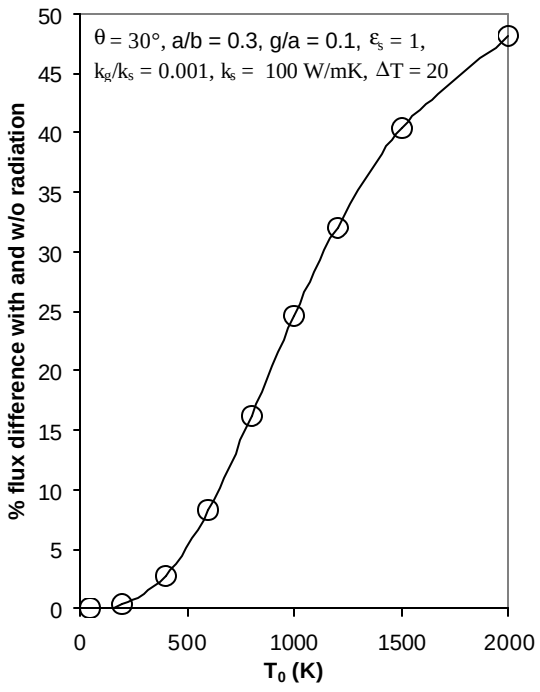

Figure 16. Variation with base temperature of the effect of radiation on the uncoated asperity.

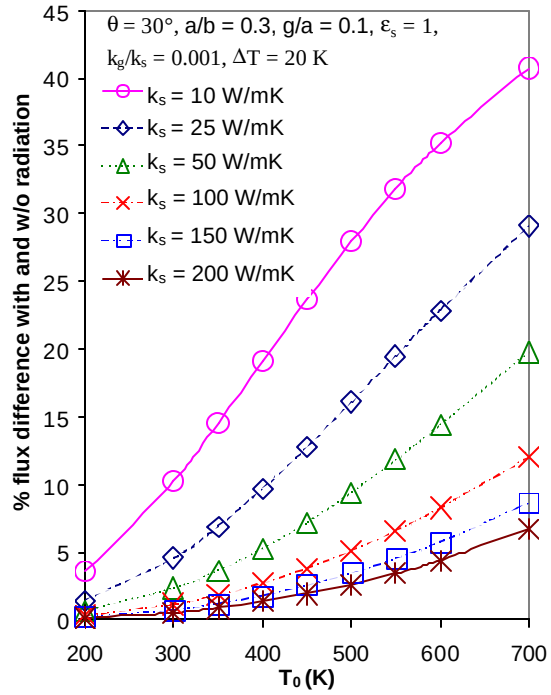

(a)

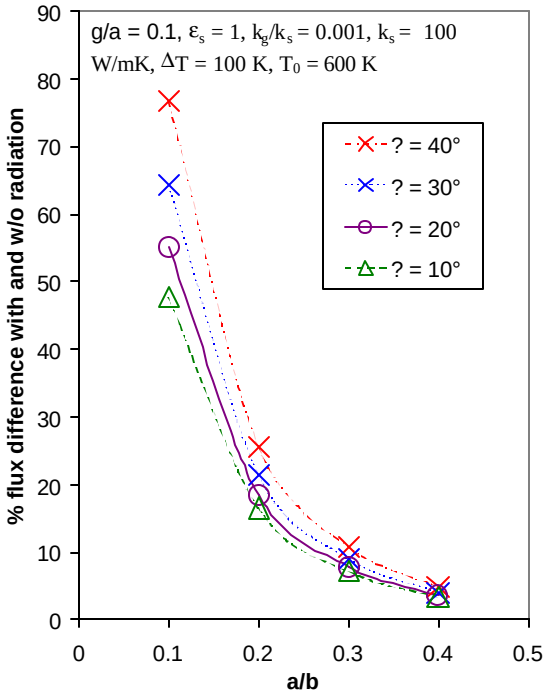

(b)

Figure 17. Variation of the effect of radiation on the uncoated asperity with (a) substrate thermal conductivity, and (b) asperity geometry.

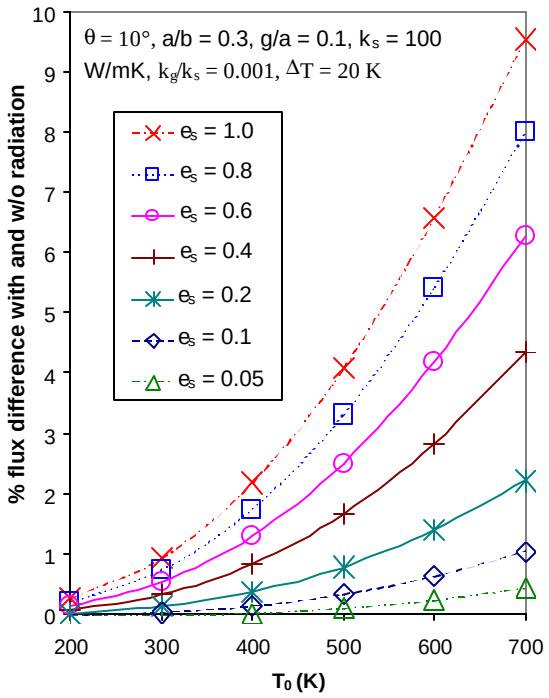

Figure 18. Variation with emissivity of the effect of radiation on the uncoated asperity.

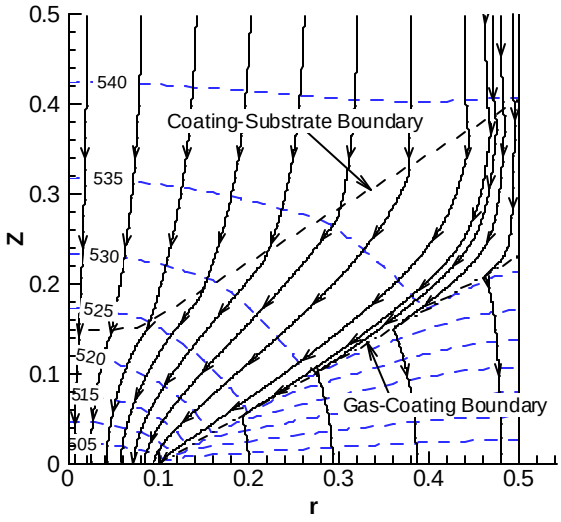

Figure 19. Temperature distribution in coated asperity with radiation (θ = 30°, a/b = 0.2, g/a = 0.1, ε_s = 1.0, k_g/k_s = 0.001, k_s = 100 W/mK, ΔT = 100 K, T_0 = 500 K, t/b = 0.3, k_c/k_s = 2).

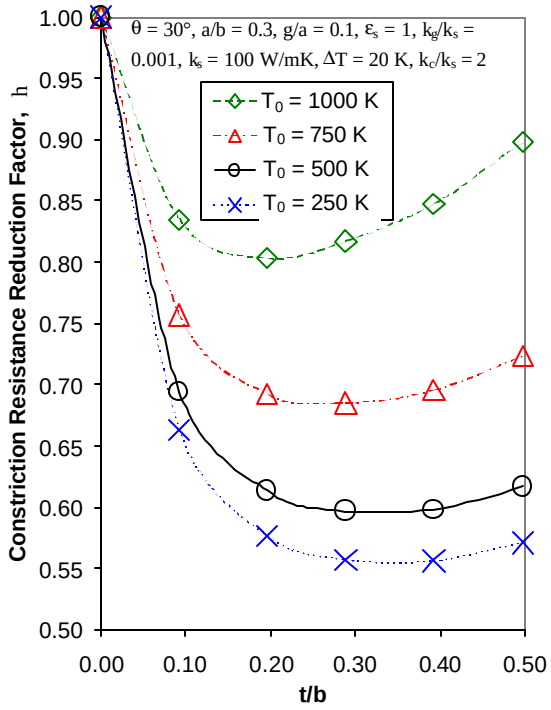

(a)

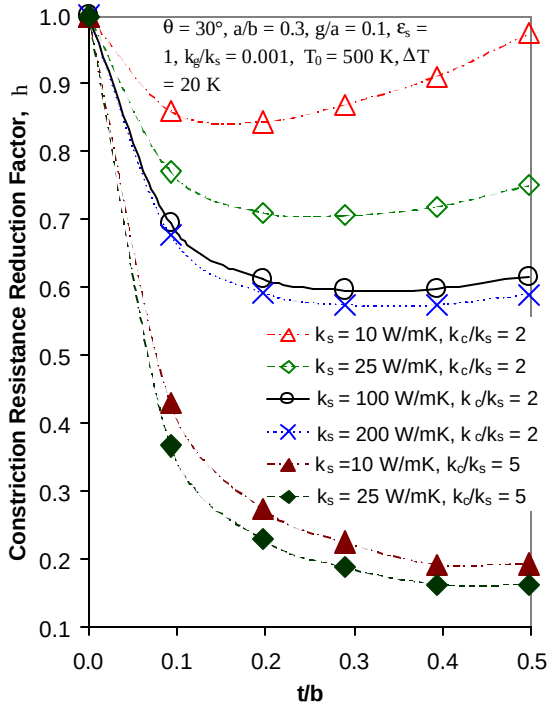

(b)

Figure 20. Variation of η versus t/b with (a) base temperature, and (b) thermal conductivities of the substrate and coating.

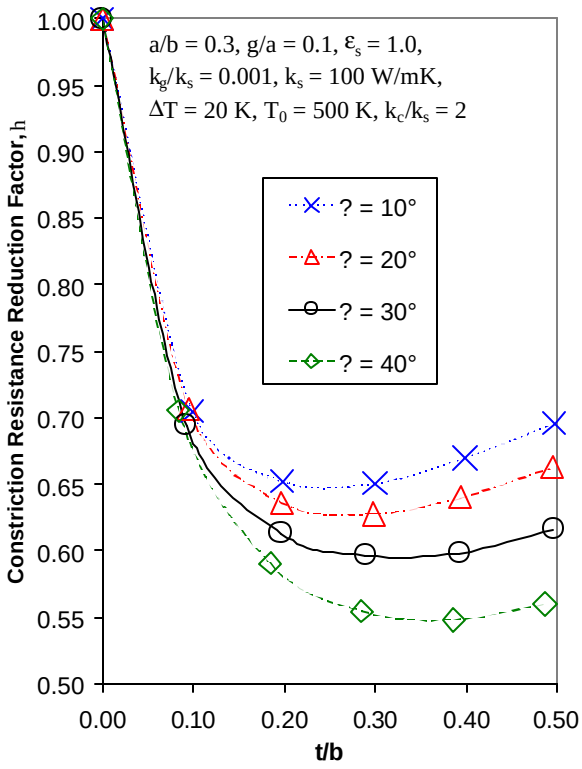

Figure 21. Variation of η versus t/b with cone angle.

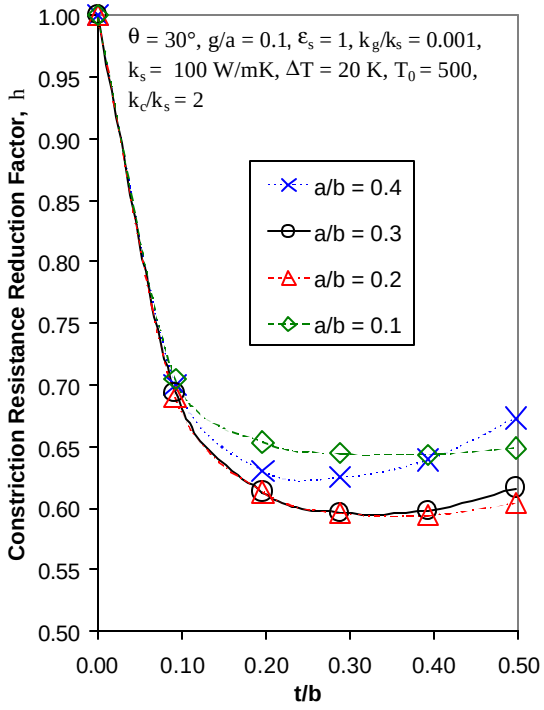

Figure 22. Variation of η versus t/b with constriction ratio.